ELSEVIER

Cement and Concrete Composites **19** (1997) 223–239

0958-9465/97/$17.00

PII:S0958-9465(97)00018-8

A Study of the Damage of Subway Structures during the 1995 Hanshin–Awaji Earthquake

Senzai Samata,[a] Hajime Ohuchi[b] & Takashi Matsuda[b]

[a]Technical Division of Rapid Transit, Department of Transportation, Kobe City, 6-5-1 Kanou-cho, Chuo-ku, Kobe 650, Japan
[b]Technical Research Institute, Obayashi Corporation, 4-640 Shimokiyoto, Kiyose, Tokyo 204, Japan

Abstract

During the 1995 Hanshin–Awaji earthquake, underground subway structures suffered significant damage, including middle column shear failure which has never been experienced in the past. The present paper describes analytical studies for damage verification and for failure mechanism investigation. Focusing on box culvert structure with middle columns at Kamisawa station, Kobe city municipal subway, the following three series of analytical studies have been conducted. In the first study, soil deposit dependent ground response are investigated using equivalent linear response analysis computer program based on multi-reflection theory. The increase of the deposit layer thickness provides less acceleration, but more displacement responses, which causes more in the way of damage in the present underground structure. In the second study, structure and ground responses are investigated with using two-dimensional soil–structure interaction computer program. As a result, the horizontal motion dependent flexural shear section force has more of an effect, but the vertical motion dependent axial force has less of an effect on the middle column damage. That section force is more affected by displacement amplification of ground dependent on deposit layer. In the third study, three-dimensional FE static nonlinear analysis is conducted to investigate failure mechanism of the damaged structure subjected to earth pressure load, which is obtained in the second study. Analytical results predict shear failure of the top story middle column prior to the flexural yielding of the slabs and walls. © *1997 Published by Elsevier Science Ltd. All rights reserved.*

INTRODUCTION

The 1995 Hyogoken–Nanbu earthquake caused severe damage in the reinforced concrete underground subway structures, which have never been experienced in the past.[1] The damage of the underground subway structures are illustrated in Fig. 1. At Daikai station, Kobe rapid transit, the structure collapse caused severe depression of the upper roadway.[2] At Kamisawa station of Kobe city municipal subway, about 400 m north of Daikai station, severe damage was also suffered in the west part of station, whilst there was less damage in the east.[3] In the Kobe city municipal subway, Shin-Nagata and San-No-Miya station structures suffered similar significant damage.

Among them, the present study focuses on the damage at Kamisawa station. It consists of the following three parts.

(1) Stratum depth dependent ground response is studied by the multi-reflection theory with equivalent linear procedure. The relationship is discussed between obtained ground response and observed damage.
(2) Focusing on both significantly and less damaged structures, acceleration, displacement and section force responses are evaluated by two-dimensional FE dynamic response analysis.
(3) Failure mechanism is studied by a three-dimensional static FE nonlinear analysis with peak earth pressure obtained in the dynamic response analysis. Predicted

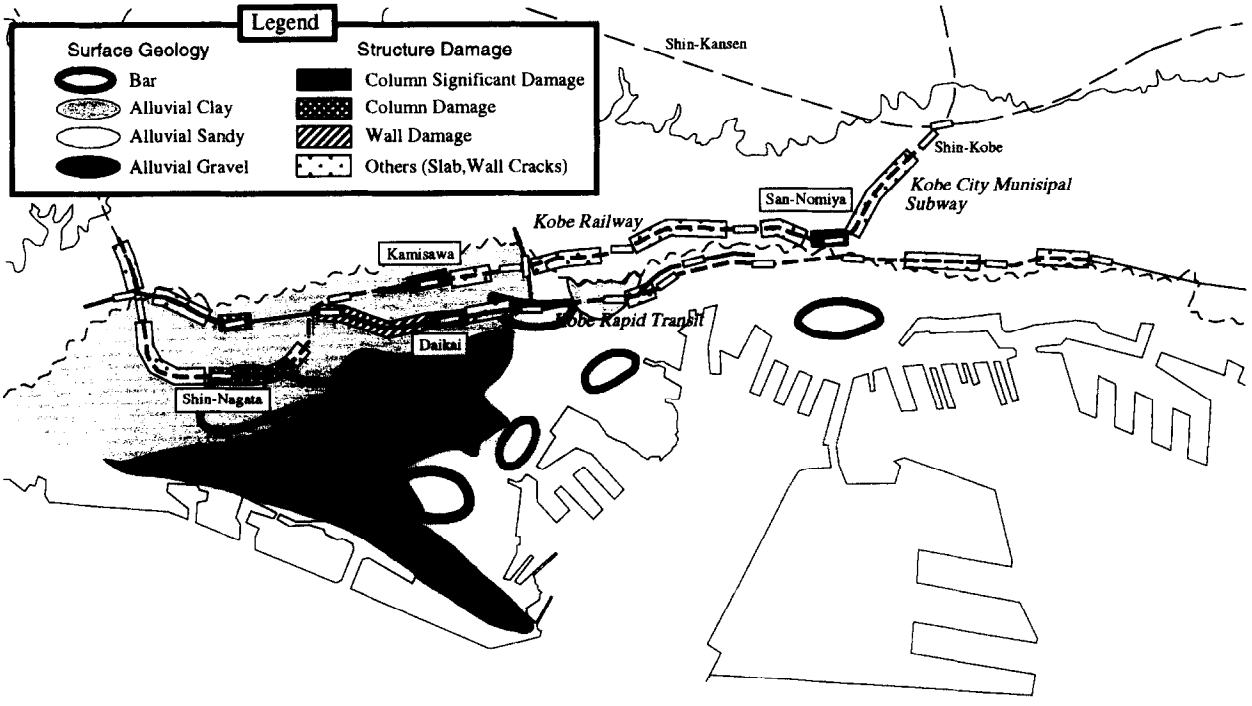

Fig. 1. Damage distribution of underground subway structures in Kobe.

shear force is then compared with code specified shear strength.

DAMAGE SUMMARY AND GEOLOGICAL PROFILE AT KAMISAWA STATION

Structures and damages[3]

Kamisawa station distributes 400 m length east to west and cross-section structure is roughly classified into two types, i.e. two span–two story and two span–three story structures. The structure is a unsymmetric box frame along a platform area, while it is symmetric in another area. Especially in the west part, with heavy damage observed, middle columns are eccentrically allocated to the south dividing the slab into a two to one span ratio.

Plan and elevation views are provided with observed damages in Fig. 2. The damage is concentrated in the west part of Nagata station. More significant damage is observed in the top story as opposed to the bottom story. Among these, 10 columns were classified as rank I, the most significant damage as shown in Fig. 2. 73% of the columns suffered more or less damage and the slab and wall also suffered longitudinal cracks in the railway direction.

Typical damages are illustrated for representative type-C and type-G cross-section structures in Fig. 3. At the top story, most middle columns of type-C spaced at 5 m pitch suffered rank I damage with concrete spalling and rebar significant buckling as shown in Fig. 1. In the Fig. 3(c, d), middle column reinforcement details are provided, i.e. D32 doubly spaced at 9.2 cm for longitudinal reinforcement and spaced at 12.5 and 25 cm, respectively, in the column end and intermediate parts for lateral hoops. As shown in Fig. 3(a), the middle column of the bottom story suffered similar damage, but less than that of the top story and middle slab ends suffered significant flexural cracks with upto 4 mm width along 130 m distance. Figure 3(b) represents damage profiles for type-G structure, with reinforced concrete column for top and middle story and 65 cm diameter steel tube column for bottom story. All members suffered similar damage to type-C except steel tubes.

Geological profile

Subsurface geology at Kamisawa station is illustrated in Fig. 4. It consists of an alluvial clayey deposit and the upper part of the subway structure is in relatively soft material, while the lower part is in the stiff soil layers. In the figure, A to Q expresses structure types, where type-C and G structures suffered the most severe

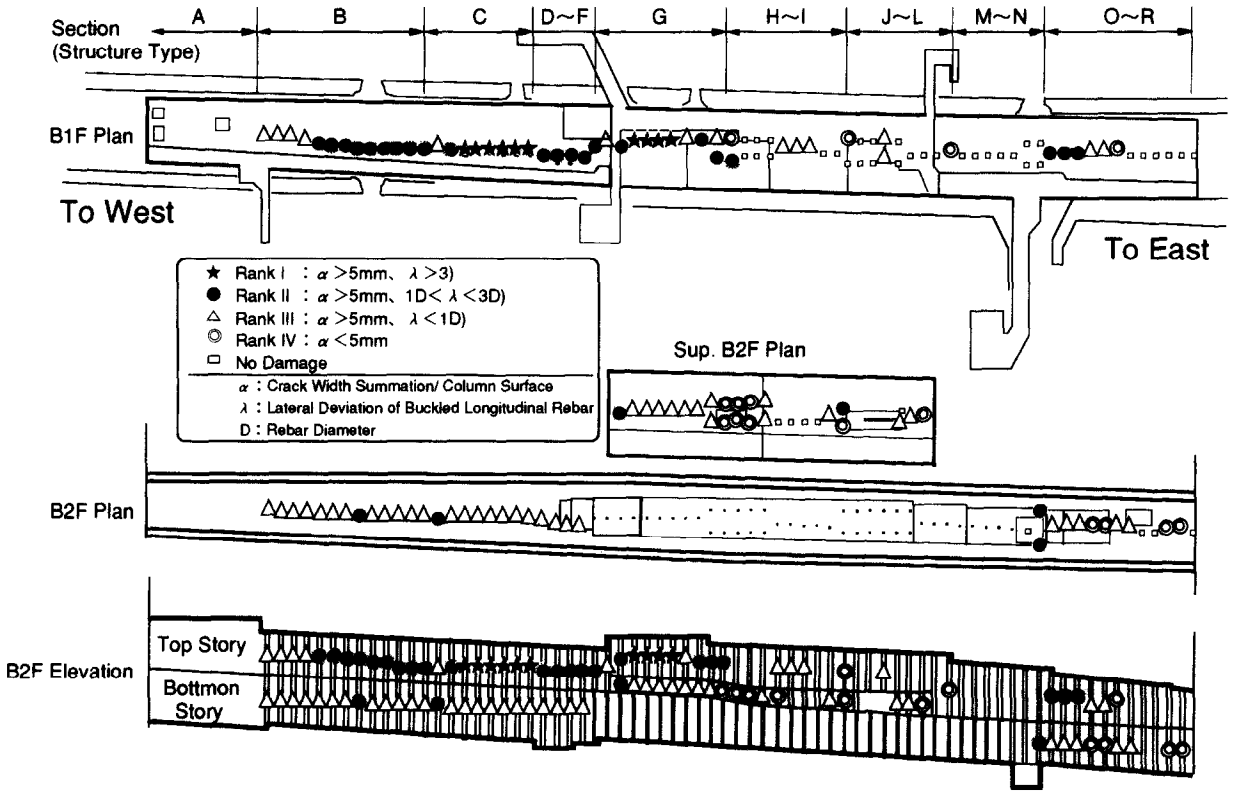

Fig. 2. Damage summary of middle column at Kamisawa station.

damage, as previously described. The west part of Kamisawa station, where the heavy damage is concentrated, is on the thicker soft deposit than the east part.

GROUND RESPONSE

Analytical model

Focusing on the transverse response of subway structure shown in Fig. 4, it is assumed that each soil layer uniformly deposits in that direction. The soil profile is tabulated in Table 1 for each section. A multi-reflection theory-based computer program 'SHAKE' is utilized for ground response analysis, where soil material nonlinearity is taken into account by equivalent linear method. Material constants are tabulated in Table 2. Dynamic characteristics are determined based on the N-value as follows:

(1) S wave velocity by Imai's equation[4] (eqn 1);
(2) initial shear stiffness G_0;
(3) friction angle ϕ by Roadway design specification[5] (eqn 2);
(4) shear strain γ_r for Hardin–Drnevich model from ϕ and G_0 (eqn 3);
(5) assumption of maximum damping factor with 25% for sand and 15% for clay and of minimum that with 2% (eqn 4).

$$Vs(c) = 114N^{0.294}, Vs(s) = 97.2N^{0.323} \quad (1)$$

$$\phi = 15+(15N)^{0.5} \quad (2)$$

$$\gamma = \sigma_m' \tan[\phi] G_0 \quad (3)$$

$$G = G_0/(1+\gamma/\gamma_r),$$

$$h = h_{min}+(h_{max}-h_{min})/(1+\gamma_r/\gamma) \quad (4)$$

As the input wave, acceleration recorded at the 83 m deep point of Port Island, Kobe (GL-83 m) is employed, that is practically considered as the basement (Vs = 320 m/s). The principle wave, consisting of both horizontal components, is input as 2E from the basement, where a maximum acceleration amplitude of E is 305 gal (Fig. 5(a)). The Fourier spectrum is represented in Fig. 5(c), where it is dominant at a frequency range of around 0.8 and 3 Hz. In the figure, vertical motion is also provided, which will be utilized in the next soil–structure interaction analysis.

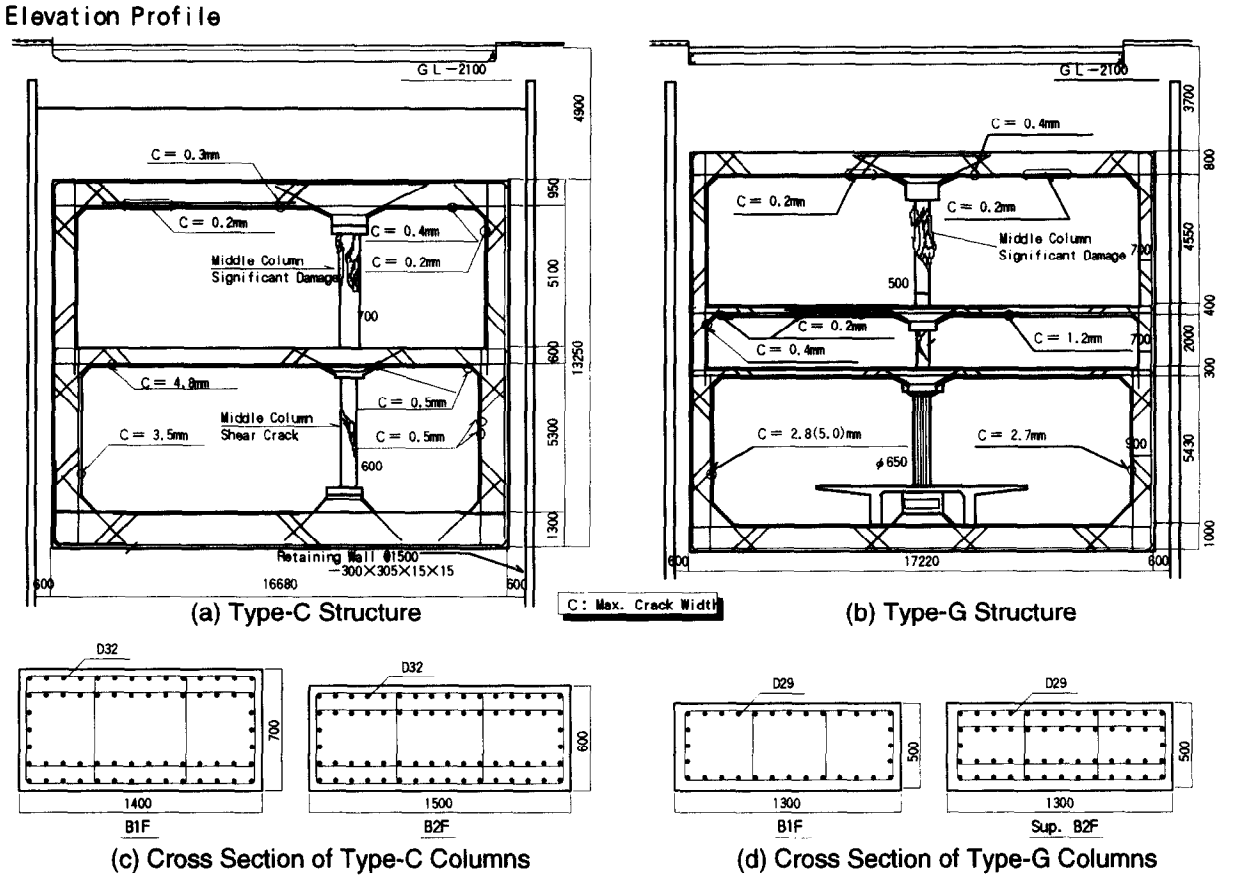

Fig. 3. Dimensions and damaged area of type-C and G structure.

Analytical results

Acceleration responses at C, G and Q section, provided in Fig. 4, are illustrated in Fig. 6 where high frequency components implied in the Q section case differ from other cases. Table 3 represents natural frequency at ground surface for each section. Linear range frequency is considered to correspond to the dynamic characteristic of ground during normal operation, while an equivalent linear case provides that during an earthquake. In the former case, the natural frequency increases from the A to Q section with a difference of at most 0.6 Hz, while in the latter case, the larger difference is observed between the A and Q sections because material nonlinearity has a greater effect during the earthquake than during normal operation.

Fig. 1. Damage view of type-C structure at Kamisawa station.

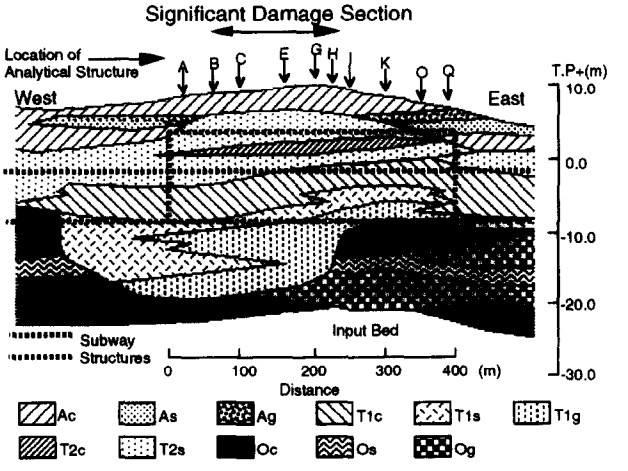

Fig. 4. Soil deposit profile of Kamisawa station

Table 1. Constitution of stratum

A		*B*		*C*		*D*		*E*	
GL(m)	*Soil no.*	*GL(m)*	*Soil no.*	*GL(m)*	*Soil no.*	*GL(m)*	*Soil no.*	*GL(m)*	*Soil no.*
−3.15	1	−2.85	1	−3.00	1	−3.30	1	−3.70	1
−3.60	2	−7.65	5	−7.65	5	−7.65	5	−7.70	5
−7.50	5	−8.40	6	−8.70	6	−8.85	6	−8.70	6
−7.92	6	−12.30	7	−11.40	7	−11.30	7	−11.00	7
−12.30	7	−17.00	8	−16.83	8	−16.20	8	−15.90	8
−16.75	8	−19.70	9	−19.60	9	−17.90	9	−17.60	9
−18.45	9	−21.90	10	−22.50	10	−26.90	10	−26.40	10
−21.00	10	−23.55	11	−23.40	11	−28.70	15	−29.40	15
−23.70	11	−27.45	12	−27.00	12	−30.20	16	−30.30	16
−27.00	12	−30.60	16	−28.10	15	–	17	–	17
−30.30	16	–	17	−30.30	16	–	–	–	–
H		*I*		*K*		*O*		*Q*	
GL(m)	*Soil no.*	*GL(m)*	*Soil no.*	*GL(m)*	*Soil no.*	*GL(m)*	*Soil no.*	*GL(m)*	*Soil no.*
−3.15	1	−3.00	1	−2.10	1	−1.50	1	−1.65	2
−3.70	2	−3.75	2	−3.30	2	−2.85	2	−3.60	3
−7.20	5	−6.75	5	−5.70	5	−4.05	3	−4.65	4
−8.65	6	−8.25	6	−7.05	6	−5.25	5	−8.30	7
−10.95	7	−10.20	7	−8.85	7	−6.15	6	−14.33	8
−13.80	8	−13.20	8	−12.00	8	−7.80	7	−16.10	10
−16.98	9	−15.75	9	−14.10	9	−11.40	8	−18.50	13
−22.70	10	−18.90	10	−17.40	10	−13.50	9	−22.80	14
−25.20	14	−22.40	13	−21.20	13	−17.00	10	−27.20	15
−29.40	15	−24.80	14	−23.20	14	−20.30	13	–	17
−30.00	16	−29.40	15	−28.40	15	−23.00	14	–	–
–	17	–	17	–	–	−27.80	15	–	–
–	–	–	–	–	–	–	17	–	–
1:ACl 6:Tc211:Tls2 16:Oc2		2:Ag 7:T2s2 12:Tlg2 17:input bed		3:As 8:tlc 13:Ocl		4:Ac2 9:Tlsl 14:Os		5:T2sl 10:Tlgl 15:Og	

Figure 7(a, b) represents peak responses, respectively, for displacement and acceleration, where the depth of the structure's lower end is at T.P.−8 m and that of upper end is at T.P.+3 m. Figure 7(b) indicates that amplification becomes larger from Q to A section in order. Figure 8 illustrates the distributions of peak acceleration and displacement from A to Q sections, where the horizontal axis indicates distance from A section to the east. At the structure's upper end, acceleration becomes larger from the A to Q section, while it is the

Table 2. Dynamic characteristics of soil

No.	*Soil legend*	*Unit weight* γ_t *(tf/m³)*	*Initial shear modulus* G_0 *(tf/m²)*	*Initialized shear strain (equation (3))* γ_r	*Max. damping ratio* h_{max}*(%)*	*Min. damping ratio* h_{min}*(%)*
1	Acl	1.80	7300	0.00200	15.0	2.0
2	Ag	1.90	15400	0.00028	25.0	2.0
3	As	1.70	6900	0.00200	15.0	2.0
4	Ac2	1.70	5000	0.00200	15.0	2.0
5	T2sl	2.00	10000	0.00047	25.0	2.0
6	T2c	1.70	8500	0.00200	15.0	2.0
7	T2s2	2.00	12600	0.00064	25.0	2.0
8	Tlc	1.70	9300	0.00200	15.0	2.0
9	Tlsl	2.00	16200	0.00088	25.0	2.0
10	Tlgl	2.10	24900	0.00088	25.0	2.0
11	Tls2	2.00	18800	0.00107	25.0	2.0
12	Tlg2	2.10	24900	0.00107	25.0	2.0
13	Ocl	1.70	14900	0.00200	15.0	2.0
14	Os	2.00	23700	0.00105	25.0	2.0
15	Og	2.10	24900	0.00113	25.0	2.0
16	Oc2	1.70	10000	0.00200	15.0	2.0
17	Input bed	2.10	40000	–	–	2.0

opposite in displacement. On the other hand, at the structure's lower end, both of them decrease from the A to Q section. The variation of response is larger at the upper part, which means that the thickness of the soil deposit has more of an effect at surface ground. Figure 9 represents peak shear strain distribution. Both in the C and G section cases, it reaches around 0.6% strain at T.P.+2 m and T.P.−3 m at which the top and bottom stories of the structure exist, respectively. This result indicates the correlationship between the observed damage and the shear strain of the ground.

Based on above analytical studies, it is found that larger displacement, but less acceleration, was imposed in the heavily damaged section. Therefore, the response of the underground structure likes to be affected by an imposed displacement rather than acceleration.

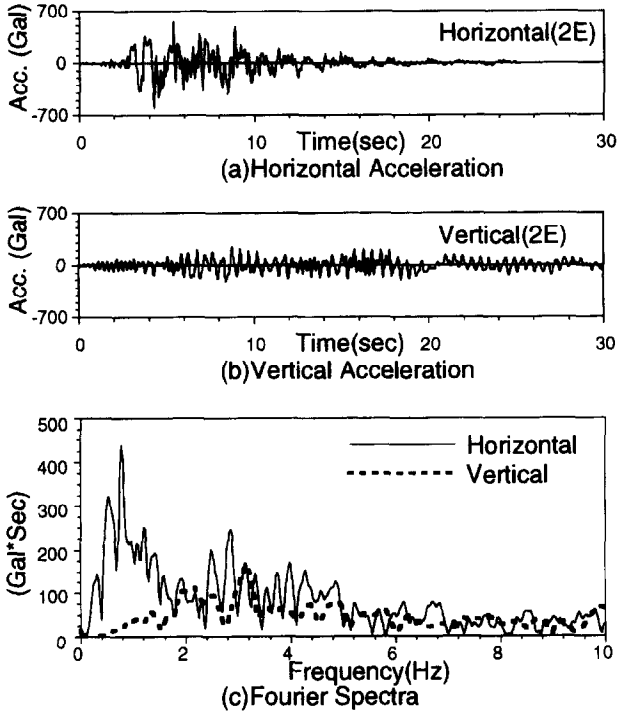

Fig. 5. Input motions from basement (2E).

SOIL–STRUCTURE DYNAMIC RESPONSE ANALYSIS

Analytical models

Focusing on the transverse dynamic characteristics of ground–structure system, the earthquake response analysis has been conducted with taking soil nonlinear behavior into account. Horizontal and vertical motion has been separately analyzed and after that obtained components are superposed. Analytical models are type-C and G structure previously shown in Fig. 3 and type-Q structure shown in Fig. 10.

The ground model is similar to that in the Section 3.1. As for the vertical motion, constant initial stiffness is assumed because amplification characteristics for vertical motion can be explained by the linear multi reflection theory for P wave based on Irikura's study.[6]

The subway structure is modeled into an assembly of beam elements assuming linear material. An equivalent cross-section, with uniform thickness, is assumed for the middle column actually spaced at 5 m pitch. Material constants are assumed as 2.4 tf/m^3 for unit weight and 5% for damping ratio. The elastic modulus is 2100000 tf/m^2 for elastic element and 55% of that for the nonlinear element considering stiffness reduction. That reduction is based on the value for a reinforced concrete member with cracks specified in JSCE concrete

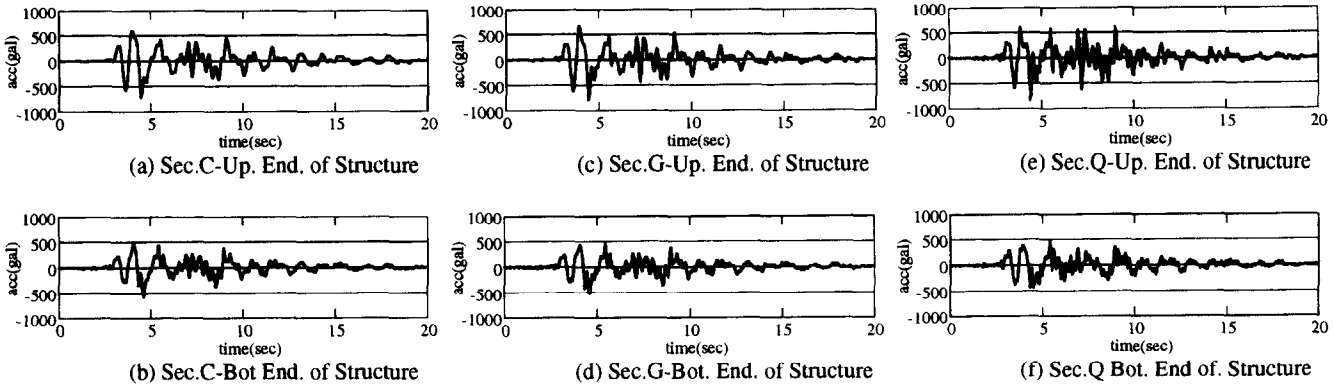

Fig. 6. Obtained ground acceleration.

design standard.[10] In the following analyses of Sections 4.2 and 4.3, no stiffness reduction of structure will be assumed (elastic structure model).

Table 3. Predominant frequencies of ground surface

Sec.	*1st frequency*		*2nd frequency*	
	Linear (Hz)	*Equivalent linear (Hz)*	*Linear (Hz)*	*Equivalent linear (Hz)*
A	2.25	1.07	5.96	2.56
B	2.27	1.17	6.03	2.78
C	2.34	1.25	6.10	2.88
E	2.39	1.32	6.25	3.03
G	2.49	1.44	6.37	3.15
H	2.59	1.61	6.54	3.61
I	2.61	1.76	6.89	4.10
K	2.73	1.93	7.13	4.59
O	2.78	1.98	7.20	4.91
Q	2.81	2.05	7.45	5.32

Damage simulation

Figure 11 illustrates the historical response of type-G structure for acceleration displacement and stresses. No significant phase difference is observed in horizontal acceleration between ground surface (F) and structure top slab (T). As for vertical response, a high frequency component appears more at the upper part with some 200 gal acceleration prior to horizontal motion.

No significant phase difference is observed in an absolute displacement between structure top slab (T) and bottom slab (U). The same are relative displacements between the top slab (T) to middle slab (M) and middle slab (M) to the bottom slab (U). From these facts, it can be said that the maximum response appears almost at same period in all parts of the structure. Of

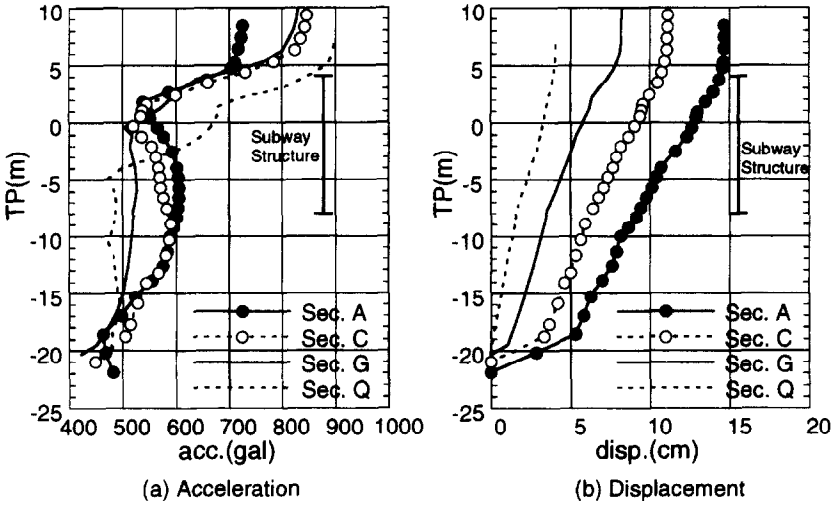

Fig. 7. Distributions of maximum acceleration and displacement to the depth.

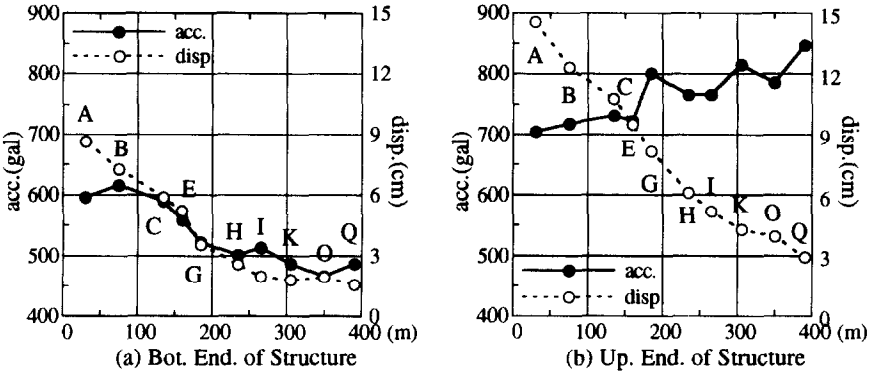

Fig. 8. Distributions of maximum acceleration and displacement to longitudinal distance.

the middle column forces, flexural moment and shear stress correlate with relative displacement, between top and bottom slabs (T−U), while axial stress with vertical acceleration at ground surface (F). Therefore, it can be said that flexural–shear behavior is deeply connected with imposed horizontal displacement and that axial behavior is affected more with vertical motion.

Figure 12 represents the historical responses for type-C and Q structures. Both structures indicate similar correlationship with type-G case shown in Fig. 11, that is, the section force is dependent on imposed displacement, but the acceleration response is independent of soil deposits and structure types.

Figure 13 illustrates peak horizontal acceleration distributions for type-C and Q structures. It is found that no significant difference is observed between the middle column and walls independent of structure configuration, symmetric or unsymmetric and that upper part of the structure indicates a larger response than the free field. The reason for the latter phenomena is that the stiffness of the structure is smaller than that of soil with same volume.

Figure 14 illustrates a maximum displacement mode for type-C and G structures. Wall deformation is similar to surrounding ground deformation, while the middle column intermediate section deforms more because of rotation restricted at the column–slab joint. Averaged shear strain of type-C and G structure middle column, which is calculated as relative displacement divided by height, attains 0.1–1.0% strain, that may cause heavy damage and at least significant cracks.

Maximum stress responses of type-C structure wall-2 are provided in Fig. 15, respectively, for permanent load, horizontal and vertical motions. The flexural–shear force is larger for horizontal motion, while the axial force is larger for permanent load. Figure 16 provides superposed stresses consisting of absolute values of the above components, i.e. permanent, horizontal and vertical components. In the figure, the flexural moment value is provided by a unit length for wall and by a column for the middle columns. Significant stress is observed at the middle column of the top story.

Normalized section forces, defined as applied force divided by strength, are illustrated in Fig. 17, where shear strength is calculated based on JSCE design standard[10] and axial strength by $fc = 210\ \mathrm{kg/cm^2}$. The member element, with more than one value for the above section

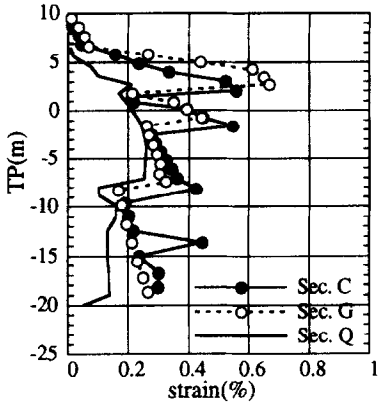

Fig. 9. Distributions of maximum shear strain to the depth.

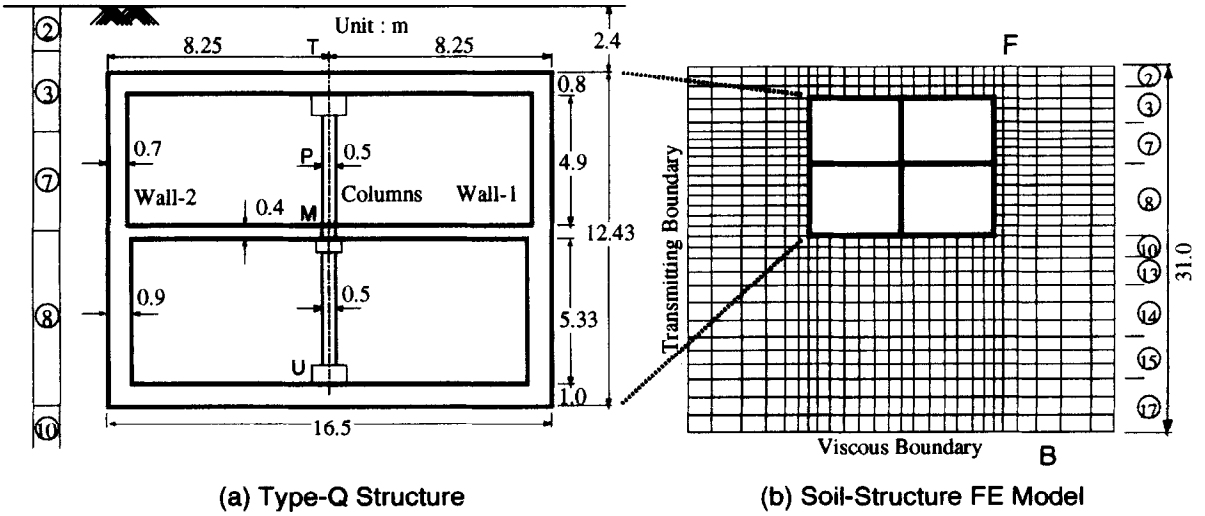

(a) Type-Q Structure (b) Soil-Structure FE Model

Fig. 10. Finite element model for soil–structure interation analysis.

force, likes to be in plastic or failure. Figure 17(a) for type-C structure suggests plastic behavior at the middle column end and the wall bottom end and critical shear failure at the top story middle column. No significant shear force acts at walls and slabs with some flexural cracks. Figure 17(b) for type-G structure provides similar section force distribution, that suggests more significant and critical shear force at the top story middle column than at the bottom story with a 1.2 value for normalized shear force. Coinciding with these observations, Fig. 17(c) for type-Q structure provides less section forces.

As described above, type-C and G structures, respectively, with unsymmetric and symmetric configuration, have been verified as critical in shear failure with the top story middle column, which is coincident with the actual damage. In addition, as described Section 3, the ground response dependent damage difference has been also verified between type-G and Q structures both with symmetric configuration.

Influence of input motion

Relationship between section force response and input motion has been studied using the type-G structure. Figures 18 and 19 represent some results of the ground response analysis previously described in Section 3. Figure 18 provides acceleration and displacement distribution of free field with variation of input motion. Figure 19 also provides the relationship between the base input motion and the response of the upper ground part, of which depth is the same as that of the structure top. With an increase of input motion, acceleration response at ground surface proportionally increases for upto 350 gal input. However, the increasing rate is becoming less for further

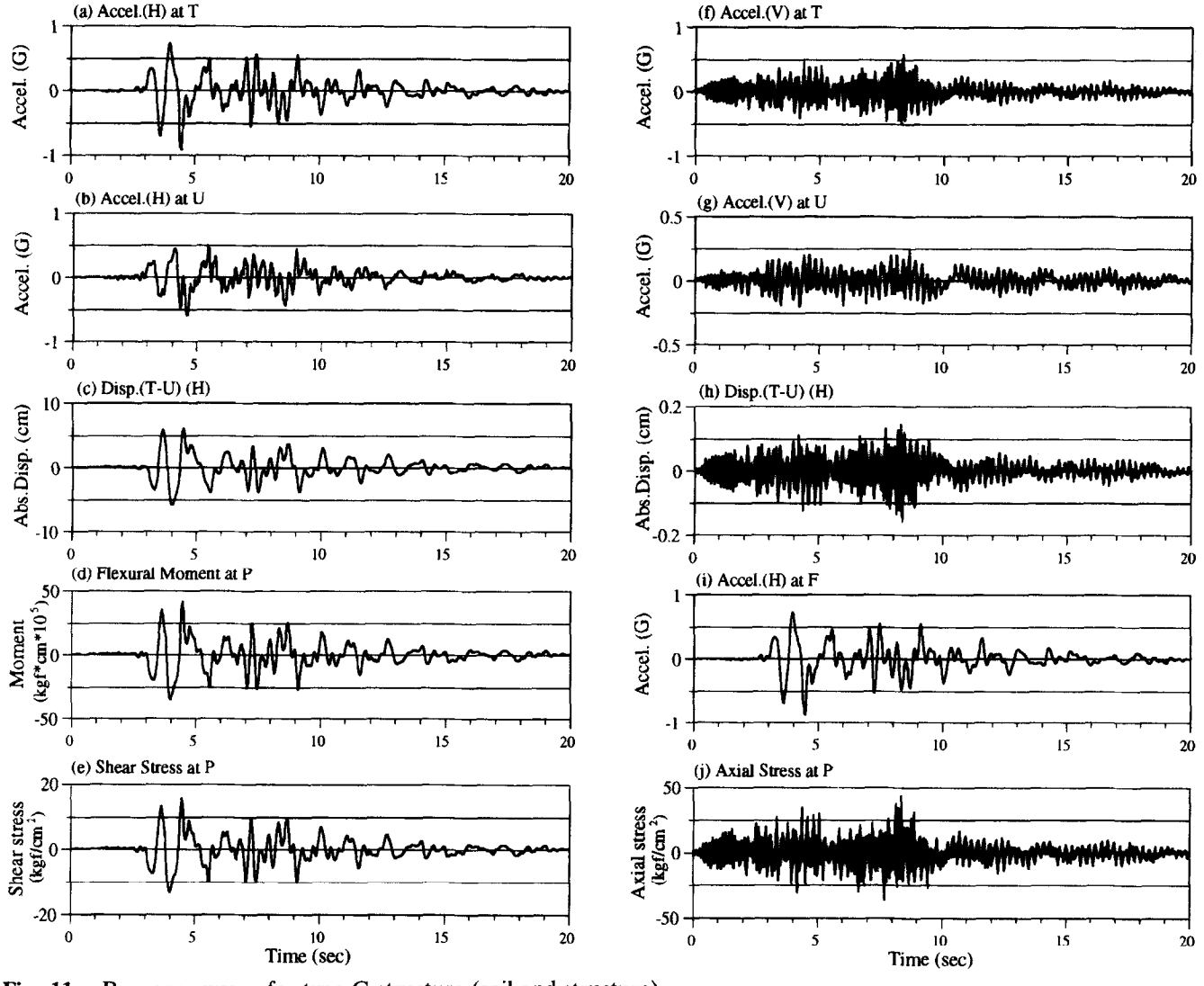

Fig. 11. Response waves for type-G structure (soil and structure).

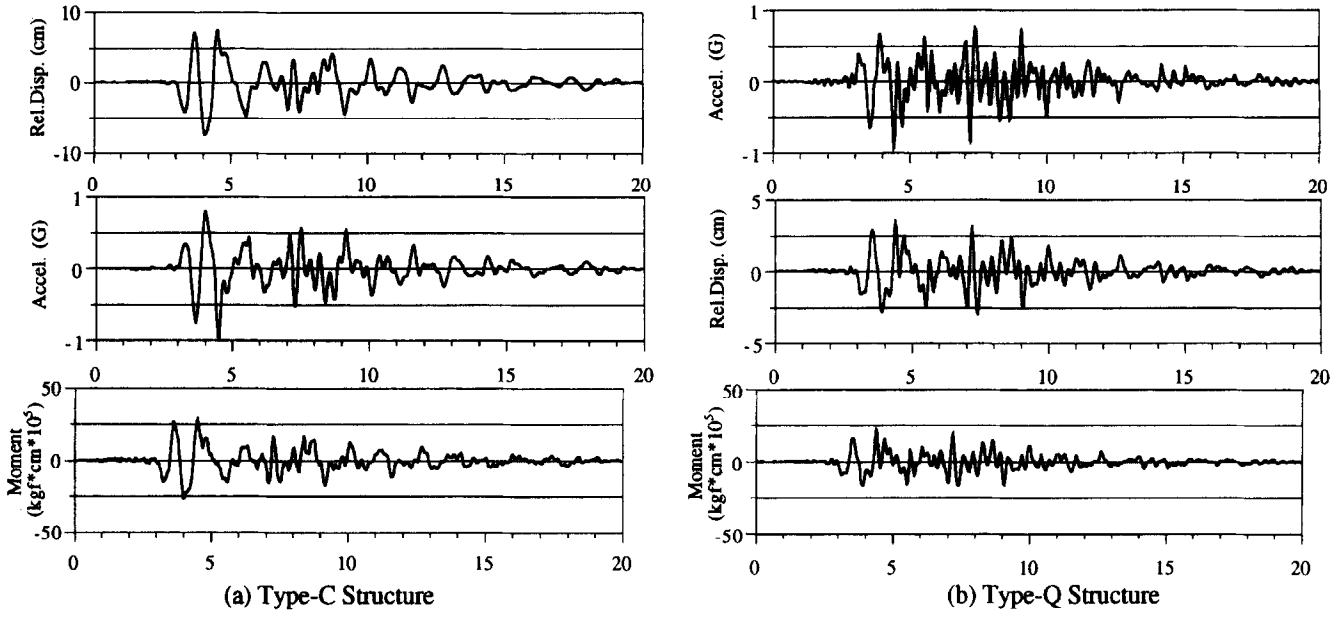

Fig. 12. Correlationship between ground and structure responses.

range until at most a 950 gal response. As for displacement, it exponentially increases with 2.86 as an exponential coefficient. Figure 20 provides the middle column normalized flexural moment and shear stress due to input motion. With less than a 300 gal input, the above section forces become less than 1 and that ensures no structure failure. Peak ground response is 500 gal against the above critical input motion of 300 gal.

Stiffness reduction of structure

Figure 21 illustrates flexural yielding section of type-G structure in comparison with observed crack regions. Here 'flexural yielding' is defined by more than 1 normalized flexural moment as shown in Fig. 17. The cracked structure, in which stiffness of the elements at the above-described yielding section is reduced to 55% of the initial, is additionally analyzed for comparison.

Figure 22 represents the middle column section force responses for both the elastic structure model and the stiffness reduced structure model. These section forces, especially shear force is remarkably less in the stiffness reduced structure than the elastic stiffness structure. Here, it should be noticed that the acceleration and displacement response of the

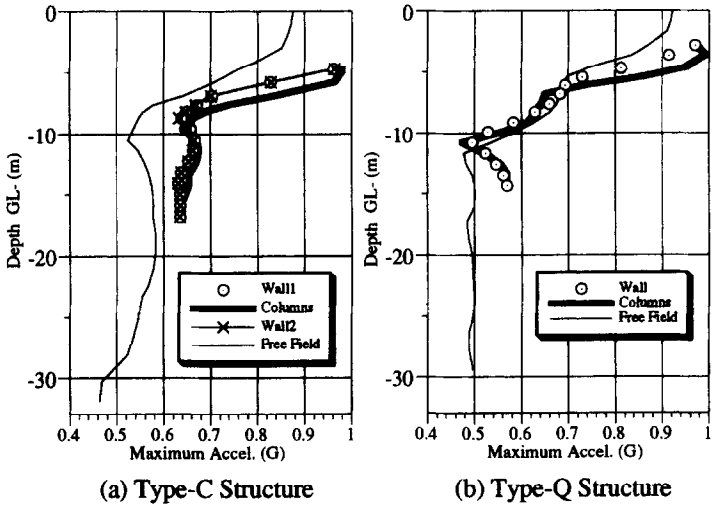

Fig. 13. Distributions of maximum acceleration to the depth.

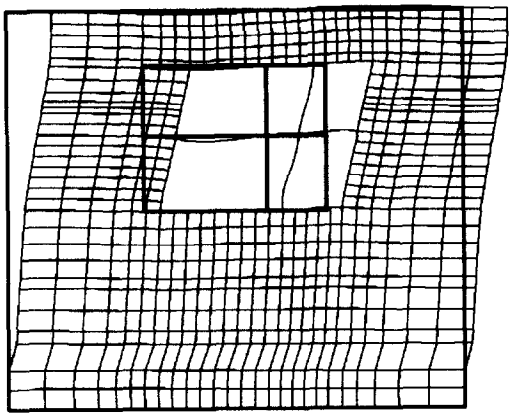

(a) Type-C Structure

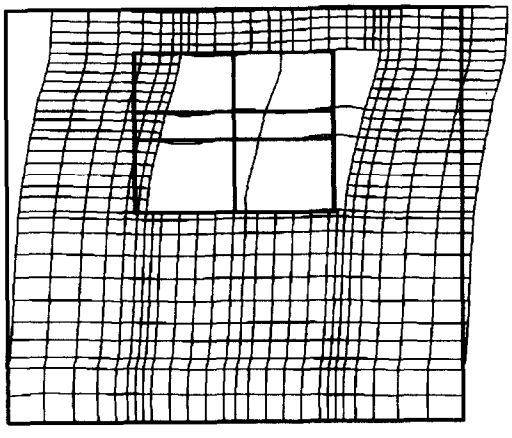

(b) Type-G Structure

Fig. 14. Displacement mode at peak.

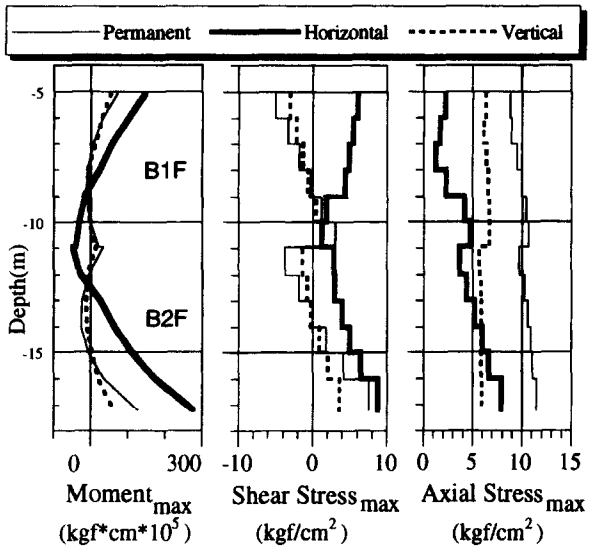

Fig. 15. Wall 2 section force distribution to the depth (type-C structure).

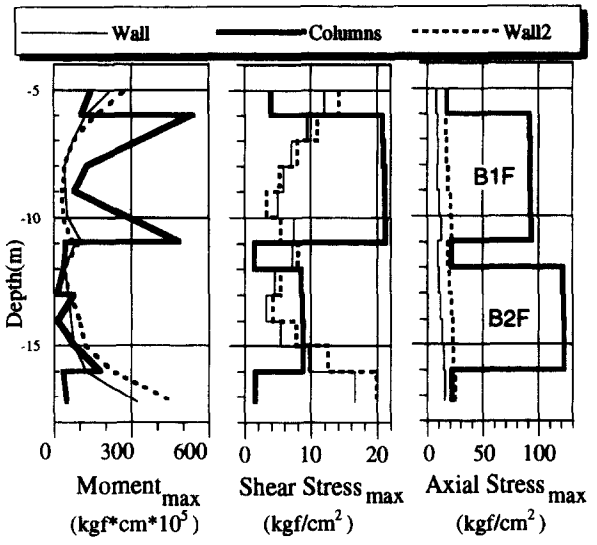

Fig. 16. Distribution of superposed section force to the depth (type-C structure).

structure is not affected by the present stiffness reduction. Figure 23 represents the comparison of the normalized section force of the middle column. The stiffness reduced structure model predicts less section force and less damage.

Through these analytical studies, it can be said that equivalent linear response analysis is effective for predicting structure nonlinear behavior with heavy damage. However, structural nonlinear behavior, especially in the ultimate range, is actually affected by redistributed stress history. This effect should be taken into account, especially for predicting the failure mechanism of the structure. This topic will be studied in the following section.

NONLINEAR FINITE ELEMENT ANALYSIS

Analytical model

Failure mechanism will be studied with earth pressure obtained in the previous dynamic response analysis. Three-dimensional finite element nonlinear static analysis has been conducted, where a slab–wall–column structure is modeled into an assembly of reinforced concrete plate elements as shown in Fig. 24. The element section force is determined as integrated stresses of each layer on the basis of plane remain assumption and two-dimensional constitutive law. For concrete stress–strain relationship, cracking is modeled as tension cut off model, while compressive behavior is by Saenz model[7] up to peak stress and as Darwin–Peck-

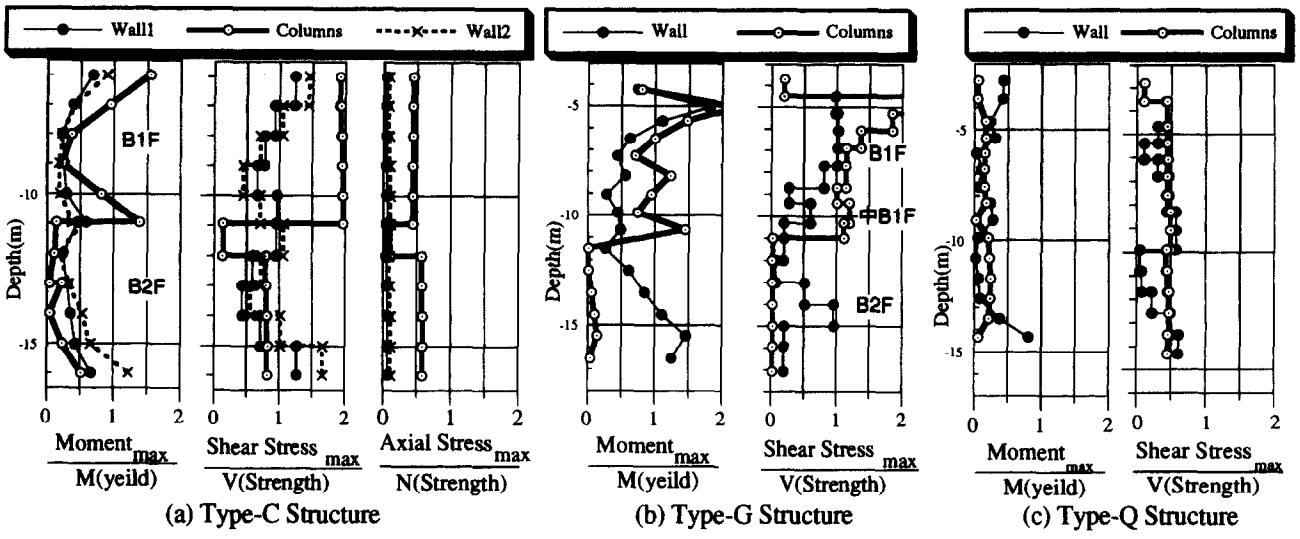

Fig. 17. Distribution of normalized section force (section force divided by strength).

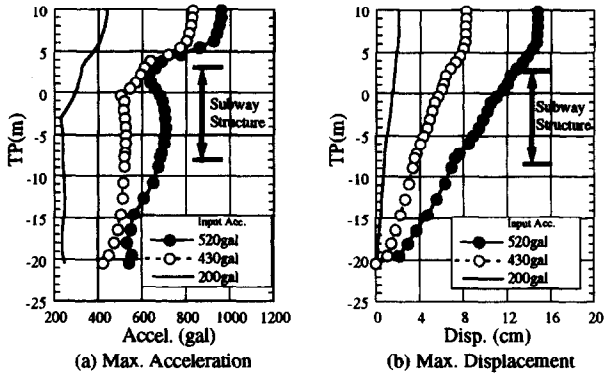

Fig. 18. Acceleration and displacement distribution dependent on input motion.

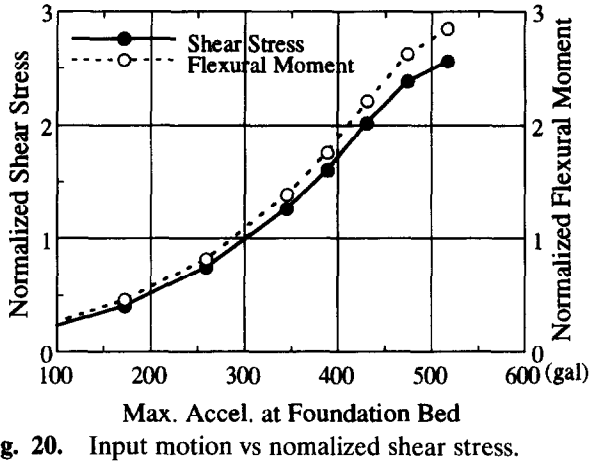

Fig. 20. Input motion vs nomalized shear stress.

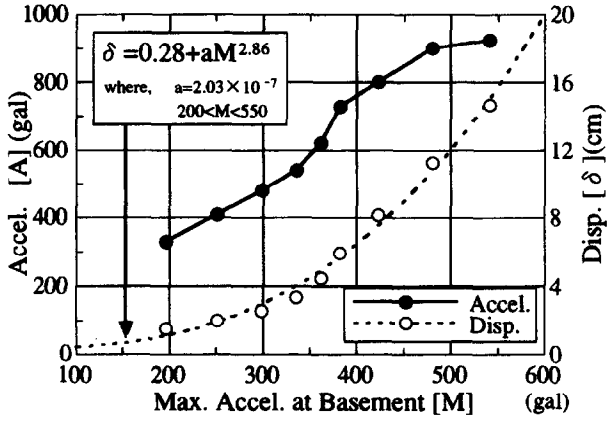

Fig. 19. Input motion vs maximum response.

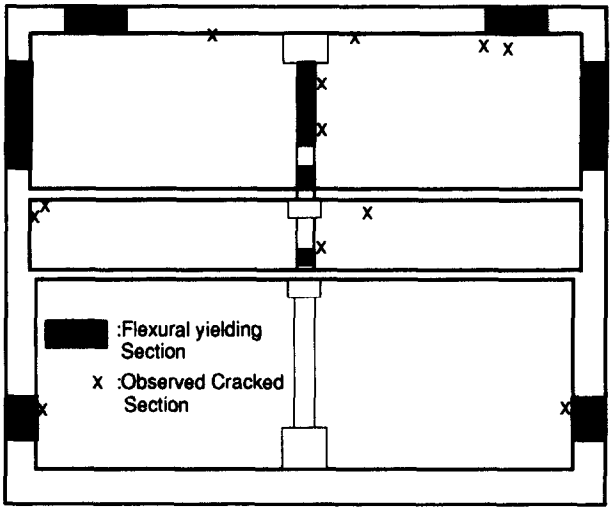

Fig. 21. Stiffness reduction sections due to cracks and yieldings (type-G structure).

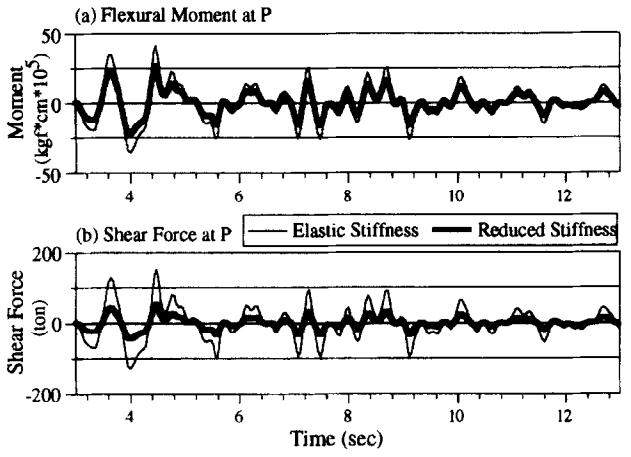

Fig. 22. Comparison of response waves between linear and equivalent linear analysis.

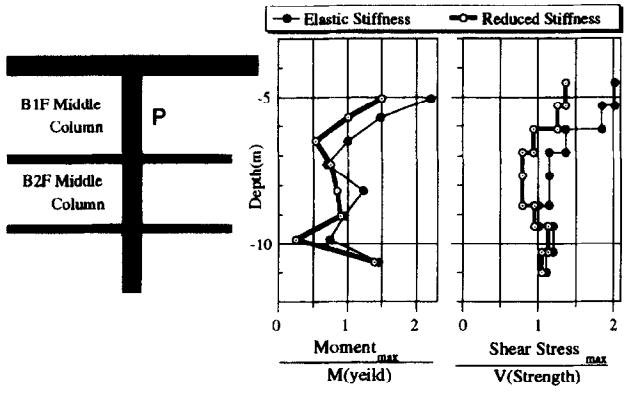

Fig. 23. Comparison of nomalized section force.

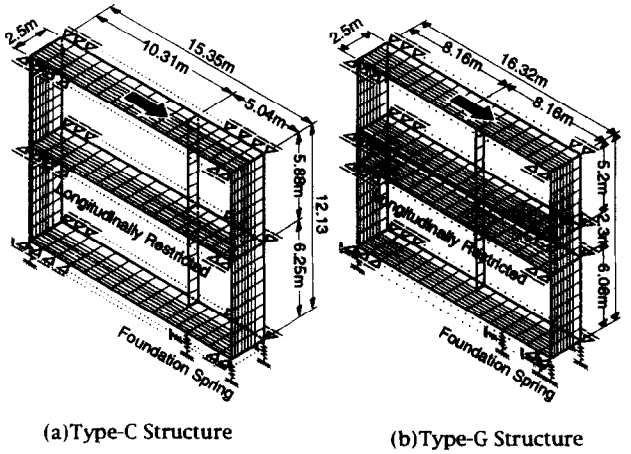

(a)Type-C Structure (b)Type-G Structure

Fig. 24. FE model for three-dimensional nonlinear static analysis.

nold model[8] in the softening region. As for concrete failure criterion, Kupfer–Gerstle model[9] for bi-axial compression stress state and Darwin–Pecknold model for tension–compression are, respectively, employed, while for bi-axial tension, cracking is assumed when maximum principal stress reaches the uniaxial tensile strength. As for steel reinforcement, elastic perfectly plastic behavior is assumed for both tensile and compressive regions. The following material constants are assumed; $fc = 250$ kgf/cm^2, $ft = 25$ kgf/cm^2 and $Ec = 260\,000$ kgf/cm^2 for concrete and $f_{sy} = 3500$ kgf/cm^2 and $Es = 2\,000\,000$ kgf/cm^2 for both longitudinal reinforcement (D32) and lateral hoop.

Analytical structures for type-C and G are modeled as shown in Fig. 24. Because of that, walls and slabs are considered to be in a plane strain state and that intermediate columns are in a plane stress state, unit structure, which consists of these members, is modeled. Applied loads are self weights and earth pressure as distributed permanent loads and then earthquake load as proportionally incremental earth pressure (Fig. 25), which is obtained in the previous dynamic response analysis. As for the latter earthquake load, earth pressure in direction from long span to short span of the slab is employed when lateral deformation of column becomes maximal.

Analytical results

Type-C structure

The shear stress histories of the walls and the middle column are compared with code specified strength[10–12] in Figs 26 and 27, where wall stress is provided as an averaged one, i.e. applied shear force divided by a cross-section area. The horizontal axis is provided in the non-dimensional form as P/Pmax, i.e. the applied

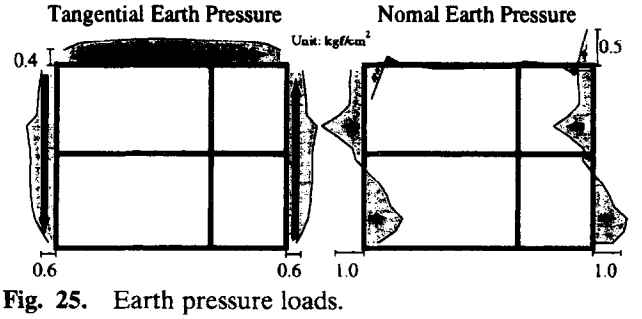

Fig. 25. Earth pressure loads.

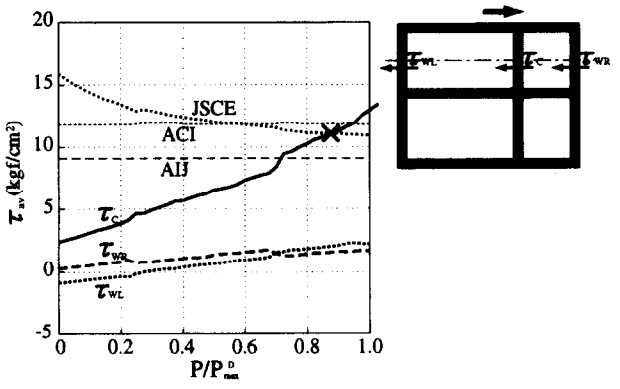

Fig. 26. Load vs shear stress relationship at top story (type-C structure).

earth pressure divided by that at maximum response obtained in the dynamic analysis. As shown in Fig. 27, the member shear stress of the bottom story is less than the specified strength. On the other hand, at the top story, the wall shear stress is, at most, about 2 kgf/cm^2, while the middle column stress reaches the JSCE specified strength at $P/P\max = 0.88$.

The shear stress distribution in the final range is provided with the deformed structure in Fig. 28. It can be found that the shear stress is significantly larger in the middle column of the top story where story shear force becomes larger than that in the bottom story, because of associated tangential earth pressure on the top slab and a normal one on the walls. Despite the dominant stresses locally observed in the middle and bottom slabs, the top story middle column is critical in shear failure.

The flexural strain distributions in the final stage are also illustrated in Fig. 29, where no yielding is observed in the reinforcement. In Fig. 30, predicted cracks on the bottom surface of the top slab is compared with the actually observed cracks. Negative loading analysis (slab short span to long span direction), separately conducted, predicts no significant crack on the focused surface, but is critical in crack initiation. These predicted phenomena almost

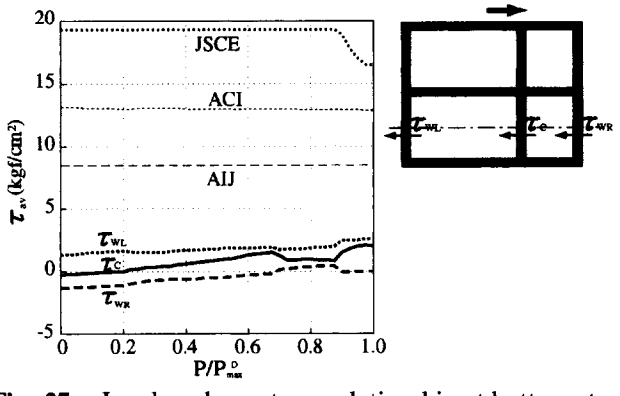

Fig. 27. Load vs shear stress relationship at bottom story (type-C structure).

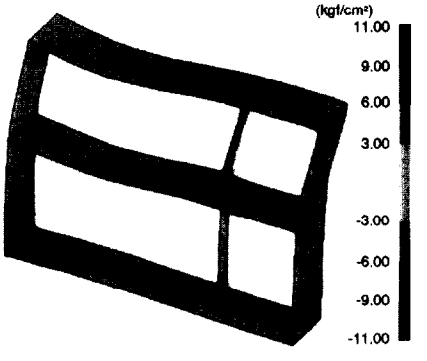

Fig. 28. Shear stress distribution at ultimate (shear failure of top story middle column.

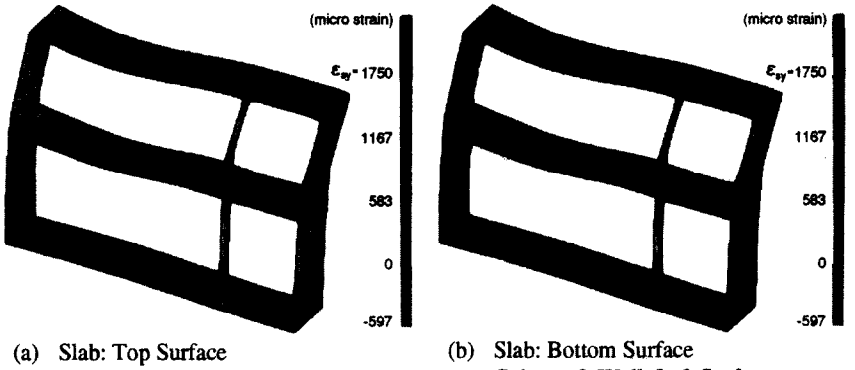

(a) Slab: Top Surface
Column & Wall: Right Surface

(b) Slab: Bottom Surface
Column & Wall: Left Surface

Fig. 29. Flexural strain distribution at ultimate (type-C structure).

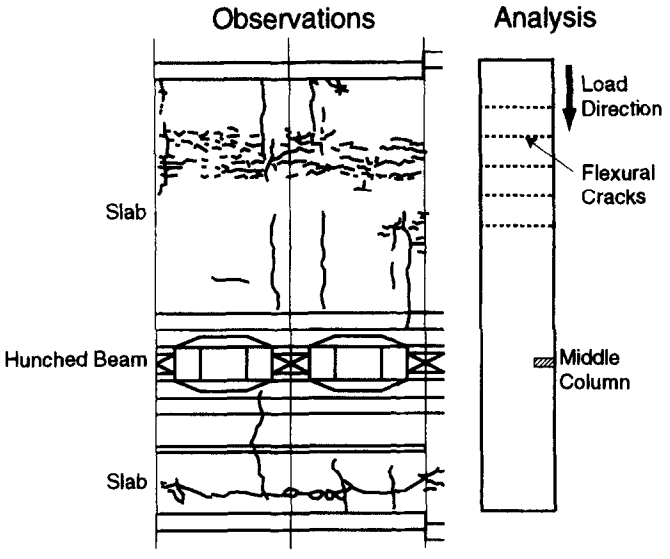

Fig. 30. Comparison of top slab damage between observations and analytical results.

correspond with the observed damage except some transverse cracks.

With this consideration, it can be said that the brittle shear failure is caused by less lateral reinforcement and significant shear force application in the middle column rigidly connected with the slabs, especially in the top story in which lateral stiffness is less and the influence of imposed earth pressure is more than that in the bottom story.

Type-G structure

In Fig. 31, similar shear stress histories of the walls and the middle column are compared with code specified strength. Less shear stress is observed in the wall, while it is dominant in the

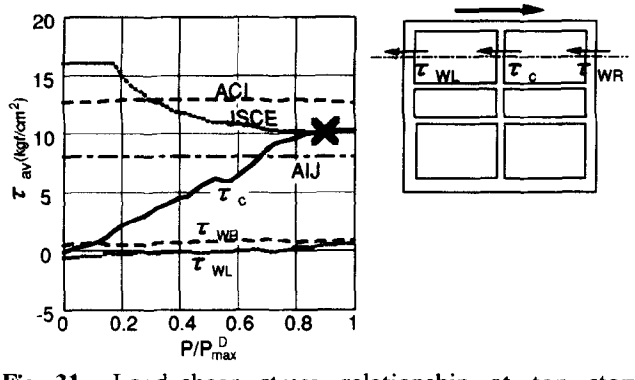

Fig. 31. Load–shear stress relationship at top story (type-G structure).

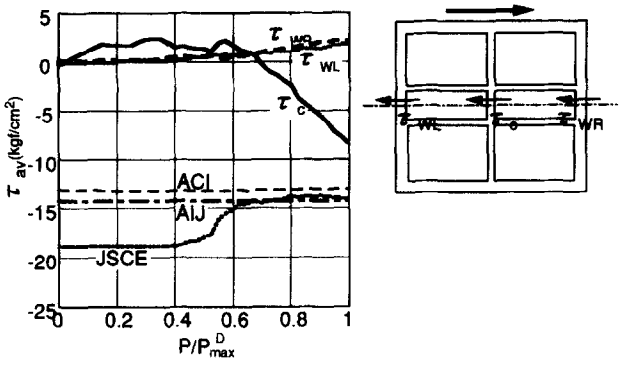

Fig. 32. Load–shear stress relationship at middle story (type-G structure).

middle column, similarly with type-C section case. Comparison with the JSCE specified strength predicts shear failure at $P/P\text{max} = 0.9$. Figure 32 represents that of the middle story column, where opposite shear force significantly increases, but does not reach shear strength. These predicted damages correspond with observations as shown in Fig. 3. As for the opposite shear force action in the middle story column, the phenomena can be explained by the variation of flexural moment gradient dependent on flexural stiffness reduction of the slabs as shown in Fig. 33. As shown in the support reaction of the illustrated continuous beam, an opposite shear force significantly acts from the top story floor slab.

The shear stress distribution in the final stage is illustrated in Fig. 34. The top story middle column is critical in shear failure even with some high stress observed in the steel column and in the floor slab of the bottom story. Figure 35 represents flexural strain distribution in the final stage, where longitudinal reinforcement yields in the upper story column top and in

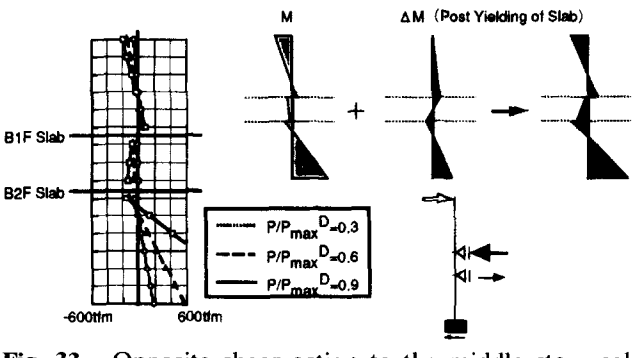

Fig. 33. Opposite shear action to the middle story column.

some walls, while all yields in the floor slab ends of the top and middle story.

CONCLUDING REMARKS

Focusing on a box culvert structure with middle columns, a number of analytical studies have been conducted for damage verification and for failure mechanism investigation. In conclusion, the following results are obtained.

(1) In the ground response analysis with soil deposit thickness taken into account, a larger displacement response is predicted in the heavier damage observed section rather than in the others.

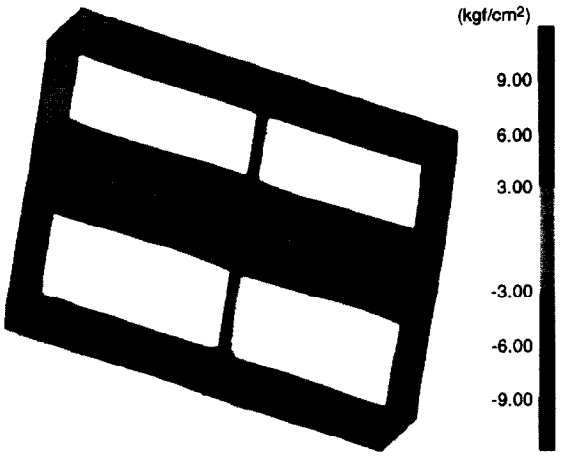

Fig. 34. Shear strain distribution at ultimate (shear failure of top story middle column of type-G structure).

(2) In the soil–structure interaction analysis, it is indicated that the response of the present underground structure is governed by the ground displacement dependent on soil deposits and that the imposed shear force on the top story middle column exceeds the specified shear strength in the case of significant damage observed structures during the earthquake. With less than 70% input motion, 300 gal at the base, which is more than the specified L1 earthquake in the present design specification, no shear failure is predicted in the above middle column.

(3) In the three-dimensional FE nonlinear analysis for two types of structures, which were heavily damaged observed in the earthquake, shear failures are predicted at both the top story middle column through a comparison of applied shear force and specified shear strength. Significant shear force is imposed on less reinforced middle column (250 mm space) of which both ends are monolithically connected with slabs, prior to the yielding of the slabs and walls.

(4) The response of the underground structure, such as the present structure is governed by ground displacement. Therefore, it is essential to ensure sufficient member ductility with prevention of brittle shear failure against imposed ground displacement. For the future seismic design of this type of underground

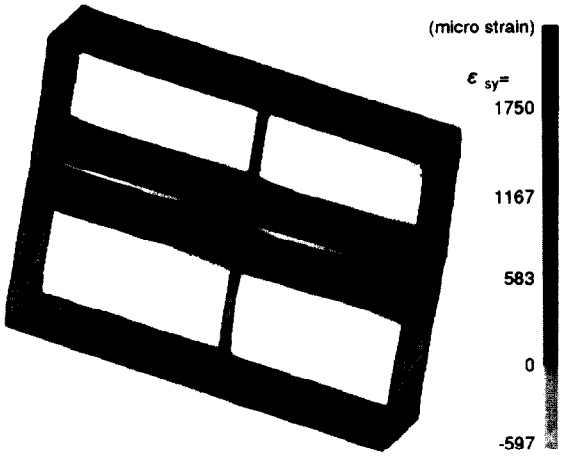

(a) Slab: Top Surface
Column & Wall: Right Surface

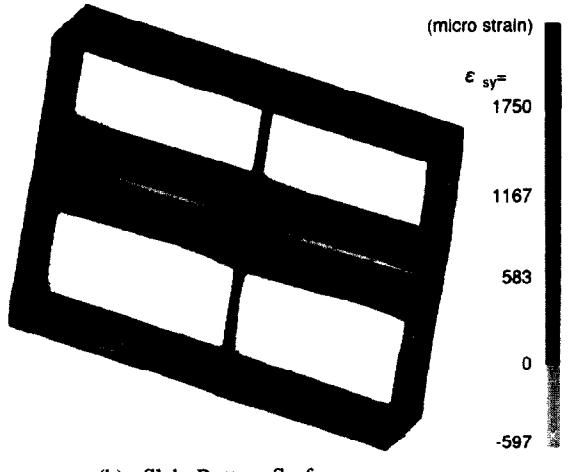

(b) Slab: Bottom Surface
Column & Wall: Left Surface

Fig. 35. Flexural strain distribution at ultimate (type-G structure).

structure, it is significant to establish a ductility design technique for the structure as well as an analytical procedure to predict correct ground displacement.

REFERENCES

1. *JSEC*, Report on the Hanshin–Awaji Earthquake, 1995, pp. 47–50.
2. Yateki, T. *et al.*, Study on the damage of Daikai station, Kobe rapid transit during Hyogoken–Nambu earthquake. In *Proceedings of JSCE*, No. 537/I-35, 1996, pp. 303–320.
3. Department of Transportation, Kobe City, Damage Summary of Kobe Municipal Subway System during Hanshin–Awaji Earthquake, 1995.
4. Imai, T., Dynamic testing method on site. *Foundation Construction*, **8** 12 (1980) 28–33.
5. Japan Roadway Association, *Design Standard and Commentary for Roadway Bridges (General Version)*, 1994, p. 199.
6. Irikura, K., Preliminary analysis of nonlinear site effects at Port Island vertical array station during the 1995 Hyogoken–Nambu earthquake. *JNDS Journal*, **16** (1995) 49–58.
7. Saenz, L. P., Discussion of equation for the stress–strain curve of concrete by Desayi and Krishnan. *ACI Journal*, **61** Sept (1964) 1229–1235.
8. Darwin, D. & Pecknold, D. A., Nonlinear biaxial stress–strain law for concrete. *Journal of the Engineering Mechanics Division, ASCE*, **103** EM2 Aug (1977) 229–241.
9. Kupfer, H. B. & Gerstle, K. H., Behavior of concrete under biaxial stress. *Journal of the Engineering Mechanics Division, ASCE*, **99** EM4 Aug (1973) 853–866.
10. *JSCE*, Concrete Design Standard, 1991.
11. *AIJ*, Ultimate strength design guideline and commentary for reinforced concrete buildings, 1990.
12. *ACI*, Building Code requirements for reinforced concrete (ACI318-83).